



Cite this: *Phys. Chem. Chem. Phys.*,
2015, 17, 8276

Complex transition metal hydrides incorporating ionic hydrogen: thermal decomposition pathway of $\text{Na}_2\text{Mg}_2\text{FeH}_8$ and $\text{Na}_2\text{Mg}_2\text{RuH}_8$

Terry D. Humphries,^{*a} Motoaki Matsuo,^b Guanqiao Li^a and Shin-ichi Orimo^{ab}

Complex transition metal hydrides have potential technological application as hydrogen storage materials, smart windows and sensors. Recent exploration of these materials has revealed that the incorporation of anionic hydrogen into these systems expands the potential number of viable complexes, while varying the counteraction allows for optimisation of their thermodynamic stability. In this study, the optimised synthesis of $\text{Na}_2\text{Mg}_2\text{TH}_8$ (T = Fe, Ru) has been achieved and their thermal decomposition properties studied by *ex situ* Powder X-ray Diffraction, Gas Chromatography and Pressure-Composition Isotherm measurements. The temperature and pathway of decomposition of these isostructural compounds differs considerably, with $\text{Na}_2\text{Mg}_2\text{FeH}_8$ proceeding via NaMgH_3 in a three-step process, while $\text{Na}_2\text{Mg}_2\text{RuH}_8$ decomposes via Mg_2RuH_4 in a two-step process. The first desorption maxima of $\text{Na}_2\text{Mg}_2\text{FeH}_8$ occurs at ca. 400 °C, while $\text{Na}_2\text{Mg}_2\text{RuH}_8$ has its first maxima at 420 °C. The enthalpy and entropy of desorption for $\text{Na}_2\text{Mg}_2\text{TH}_8$ (T = Fe, Ru) has been established by PCI measurements, with the ΔH_{des} for $\text{Na}_2\text{Mg}_2\text{FeH}_8$ being 94.5 kJ mol⁻¹ H₂ and 125 kJ mol⁻¹ H₂ for $\text{Na}_2\text{Mg}_2\text{RuH}_8$.

Received 16th January 2015,
Accepted 17th February 2015

DOI: 10.1039/c5cp00258c

www.rsc.org/pccp

Introduction

Transition metals are renowned for their diverse range of valence states and structural conformations.^{1,2} As such, in the last five decades a swathe of homoleptic transition metal hydrides have been synthesised to determine their potential for technological applications. Mg_2NiH_4 was first realised for its reversible hydrogenation properties in 1968,³ and has since been investigated for a variety technological applications including smart windows and sensors.⁴⁻⁷ Mg_2FeH_6 , with a gravimetric hydrogen storage content of 5.5 wt% has since been developed,⁸⁻¹⁴ along with a host of other transition metal hydride congeners and derivatives.^{1,2,15-22}

The transition metal hydrides of Group 8 often form octahedral $[\text{TH}_6]^{4-}$ anions, of which are limited to four-fold coordination by counterions (M) in the form of $\text{M}^+\text{M}'^+\text{M}''^+\text{M}'''^+$, $\text{M}^{2+}\text{M}'^+\text{M}''^+$, $\text{M}^{3+}\text{M}'^+$, $\text{M}^{2+}\text{M}'^{2+}\text{M}''^+$. Expanding the diversity of coordination can be achieved by increasing the anionic charge of the system, for instance by the inclusion of H⁻. A recent DFT

study by Takagi *et al.* established that the incorporation of anionic hydrogen into complex transition metal hydride compounds enables inclusion of a wider variety of cations, thereby allowing tuning of these materials in order to optimise their thermodynamic properties or hydrogen storage capacities.²³ To date, a variety of quaternary complex hydrides have been synthesised and their structural and physical properties explored, these include $\text{LaMg}_2\text{NiH}_7$ ($\text{La}^{3+}\cdot 2\text{Mg}^{2+}\cdot 3\text{H}^-\cdot [\text{NiH}_4]^{4-}$),^{18,24} $\text{Na}_2\text{Mg}_2\text{NiH}_6$ ($2\text{Na}^+\cdot 2\text{Mg}^{2+}\cdot 2\text{H}^-\cdot [\text{NiH}_4]^{4-}$),^{19,25} $\text{Na}_2\text{Mg}_2\text{TH}_8$ ($2\text{Na}^+\cdot 2\text{Mg}^{2+}\cdot 2\text{H}^-\cdot [\text{TH}_6]^{4-}$) (T = Fe, Ru),²⁰ MMg_2FeH_8 ($\text{M}^{2+}\cdot 2\text{Mg}^{2+}\cdot 2\text{H}^-\cdot [\text{TH}_6]^{4-}$) (M = Ba, Ca, Sr; T = Fe, Ru, Os)^{15,16,26} and $\text{M}_4\text{Mg}_4\text{Fe}_3\text{H}_{22}$ ($4\text{Ca}^{2+}\cdot 4\text{Mg}^{2+}\cdot 4\text{H}^-\cdot 3[\text{FeH}_6]^{4-}$) (M = Ca, Yb).^{27,28} Thermodynamic data for these materials are scarce, although some experimental^{15,28} and DFT calculated²³ values have been determined. $\text{SrMg}_2\text{FeH}_8$ and $\text{BaMg}_2\text{FeH}_8$ decompose at ca. 440 and 450 °C under 0.1 MPa H₂,¹⁵ respectively, while $\text{Ca}_4\text{Mg}_4\text{Fe}_3\text{H}_{22}$ and $\text{Yb}_4\text{Mg}_4\text{Fe}_3\text{H}_{22}$ decompose at ca. 395 and 420 °C,^{1,27,28} respectively. The enthalpy of desorption of $\text{Ca}_4\text{Mg}_4\text{Fe}_3\text{H}_{22}$ and $\text{Yb}_4\text{Mg}_4\text{Fe}_3\text{H}_{22}$ to their corresponding binary hydrides has been calculated to be 122 and 137 kJ mol⁻¹ H₂, respectively.²⁸ These values are significantly larger than those determined for the ternary Mg_2FeH_6 at 87 kJ mol⁻¹ H₂,²⁹ which decomposes at ca. 300 °C,¹³ and indicates the increased stabilisation offered by the incorporation of anionic hydrogen and varied cations into these quaternary compounds.

The isostructural compounds of $\text{Na}_2\text{Mg}_2\text{FeH}_8$ (5.1 wt% H) and $\text{Na}_2\text{Mg}_2\text{RuH}_8$ (4.0 wt% H) hold potential as hydrogen

^a WPI-Advanced Institute for Materials Research, Tohoku University, 2-1-1 Katahira, Aoba-ku, Sendai 980-8577, Japan. E-mail: terry_humphries81@hotmail.com; Fax: +81-22-215-2091; Tel: +81-22-215-2094

^b Institute for Materials Research, Tohoku University, 2-1-1 Katahira, Aoba-ku, Sendai 980-8577, Japan. E-mail: orimo@imr.tohoku.ac.jp; Fax: +81-22-215-2091; Tel: +81-22-215-2093



storage materials.²⁰ To make a fair assumption of their prospective application, a true understanding of the physical properties of these novel quaternary complex transition metal hydrides must be determined, unto which the data is extremely sparse. As a consequence, the influence of H^- on the thermal stability and decomposition process of these materials is generally unknown and must be understood. As such, *ex situ* powder X-ray diffraction (PXRD) and Pressure-Composition Isotherm Measurements (PCI) have been conducted. Their temperatures and pathways of decomposition have been established and the associated enthalpies and entropies of H_2 desorption have been calculated and compared to literature values.

Experimental

All preparation and manipulation was performed in a Miwa glove box filled with purified argon (<1 ppm O_2 and the dew point of H_2O below 190 K) to avoid contamination.

The synthesis of $Na_2Mg_2FeH_8$ was carried out by two methods: S1 followed a four step process, which first required the synthesis of Mg_2FeH_6 . This was achieved by mechanically milling (Fritsch Pulverisette 7) MgH_2 (hydrogen storage grade, Sigma Aldrich) and Fe (99.99%, Mitsuiwa) powders at a molar ratio of 2 : 1 for 2 h at 400 rpm (ball-to-powder ratio 40 : 1), under argon with subsequent heat treatment of the pelletised powder at 400 °C for 20 h under 3 MPa H_2 . The resultant olive green powder was then mechanically milled with NaH (95%, Sigma Aldrich) at a molar ratio of 1 : 2 for 20 h under argon (S1-BM) with subsequent heat treatment of the pelletised powder at 400 °C for 20 h under 30 MPa H_2 . The product was yielded as an olive green powder.

The synthesis of S2 ($Na_2Mg_2FeH_8$) followed a two-step process. NaH, MgH_2 and Fe powders at a molar ratio of 2 : 2 : 1 were mechanically milled for 20 h at 400 rpm (ball-to-powder ratio 40 : 1), under argon (S2-BM) with subsequent heat treatment of the pelletised powder at 400 °C for 60 h under 30 MPa H_2 . The product was yielded as an olive green powder.

The synthesis of $Na_2Mg_2RuH_8$ followed a two-step process. MgH_2 , NaH and Ru (99.9%, Kojundo Chemical Laboratory) were mechanically milled (identical parameters as employed with $Na_2Mg_2FeH_8$) at a molar ratio of 2 : 2 : 1 for 20 h under argon (S3-BM), before subsequent heat treatment of the pelletised powder at 500 °C for 20 h under 30 MPa H_2 . The product was yielded as a light grey powder.

Powder X-ray diffraction (PXRD) measurements were conducted using a conventional X-ray diffractometer (Lab-PXD, PANalytical X'Pert-Pro, $CuK\alpha$ radiation) in flat plate mode. Data were collected using a X'Celerator X linear position sensitive detector within a 2θ range of 10–90° using 0.02° steps at 0.04°/s with X-ray generator operating conditions of 45 kV and 40 mA. The PXRD samples were loaded in an Ar glovebox and the sample holder covered by Mylar film to prevent oxygen/moisture contamination during data collection. PANalytical HighScore Plus v. 3.0, DICVOL,³⁰ CHEKCELL³¹ and GSAS^{32,33} were used for phase identification, indexing, space group identification and Rietveld refinement, respectively.

A GC323 (Gas Chromatography) (GL sciences Inc.) was used to detect the desorbed H_2 by means of a TCD detector, with a column temperature of 200 °C. Samples were heated at a rate of 5 °C min^{-1} under an Ar flow of 40 $ml\ min^{-1}$.

Typical Pressure-Composition Isotherm Measurements (PCI) were conducted inside custom-built manometric apparatus, where the sample cell was placed in a furnace and heated to the desired temperature at a hydrogen pressure of 6 MPa or 30 MPa. The experiment was controlled by software developed by Suzuki Shokan Co., Ltd.

Results and discussion

Synthesis of $Na_2Mg_2TH_8$ (T = Fe, Ru)

The synthesis of $Na_2Mg_2FeH_8$ was first reported to utilise Mg_2FeH_6 as a starting material, which was consequently milled for 20 h with NaH (S1-BM), followed by hydrogenation at 30 MPa H_2 at 400 °C (eqn (1) and (2)).²⁰ Overall, this method is time intensive (in excess of 100 h due to the requirement of two milling and two hydrogenation procedures), and the final product also contains Fe, NaH, and Mg_2FeH_6 impurities. In order to reduce the time requirements and levels of impurities, alternative synthetic routes were investigated. It was determined that successful synthesis is achievable by ball milling $2NaH + MgH_2 + Fe$ (S2-BM), followed by hydrogenation at 30 MPa H_2 at 400 °C (eqn (3)), with an associated time requirement of 80 h. The products after milling of each material differ considerably (Fig. 1), the constituents of S1-BM, identified by PXD are not altered during milling ($Mg_2FeH_6 + NaH$) despite a broadening of the peaks due to a decrease of crystallite size (or reduced crystallinity).³⁴ The products of S2-BM were $NaMgH_3 + Fe$.³⁵

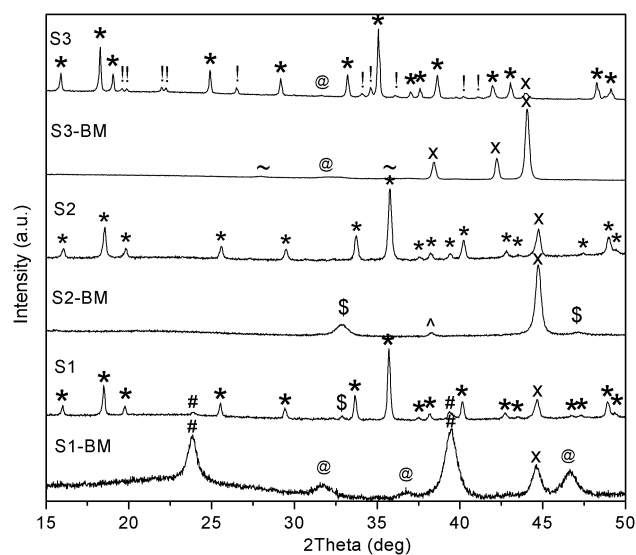


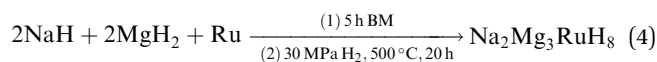
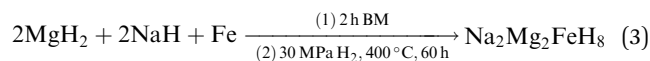
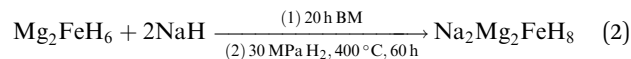
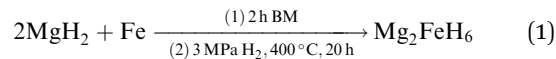
Fig. 1 PXRD of ball milled samples S1-BM ($Mg_2FeH_6 + 2NaH$), S2-BM ($2NaH + 2MgH_2 + Fe$) and S3-BM ($2MgH_2 + 2NaH + Ru$) and hydrogenated samples of S1-3. $\lambda = CuK\alpha$. * = $Na_2Mg_2TH_8$ (T = Fe, Ru); # = Mg_2FeH_6 ; @ = NaH; x = T (Fe, Ru); \$ = $NaMgH_3$; ^ = NaOH; + = Mg; ~ MgH_2 ; ! = unknown phase.



Hydrogenation of the ball milled samples S1-BM and S2-BM under standard conditions (30 MPa H₂ and 400 °C for 60 h), resulted in the formation of Na₂Mg₂FeH₈ as the major phase (Fig. 1). Analysis of hydrogenated S1 by Reitveld refinement indicates that the sample is 80.3(9)% pure and as such contains residual Mg₂FeH₆ (8.9(4)%), Fe (7.9(2)%), NaMgH₃ (2.5(3)%) and NaH (2.7(2)%) starting materials. Analysis of hydrogenated S2 indicates that the sample contains 90.6(4)% Na₂Mg₂FeH₈ and 9.4(3)% Fe, without residual Mg₂FeH₆ or NaH. This indicates that the optimal method of synthesis is *via* the S2 method due to the elimination of the prerequisite Mg₂FeH₆ synthesis (eqn (1)) and overall decrease in impurities compared to S1, primarily due to the initial (complete) formation of NaMgH₃ during the milling reaction. Milling initiates the breaking of the strong Na–H bonds, which is required to ensue during the annealing phase when synthesised *via* Mg₂FeH₆ (S1). This ultimately leads to the observation of unreacted NaH and Mg₂FeH₆ starting materials.

The synthesis of Na₂Mg₂RuH₈ follows a two-step reaction, where stoichiometric quantities of Ru, NaH and MgH₂ are milled for 5 h (S3-BM) before hydrogenation under 30 MPa H₂ at 500 °C for 20 h (S3) (eqn (4)).²⁰ The composition of the milled material is unchanged from the starting materials

(Fig. 1), whereas after hydrogenation the sample appears to be mostly Na₂Mg₂RuH₈, but also comprises of some residual Ru. An unknown material is also identifiable within the Na₂Mg₂RuH₈ powder (S3), of which only a few reflections are discernible. The occurrence of these additional Bragg peaks were also noted previously.²⁰



Thermal decomposition of Na₂Mg₂TH₈ (T = Fe, Ru)

In order to determine the thermal decomposition temperatures of Na₂Mg₂TH₈ (T = Fe, Ru), aliquots of each material were heated at a rate of 5 °C min⁻¹ with GC detecting the corresponding desorbed H₂. The chromatograms obtained (Fig. 2a)

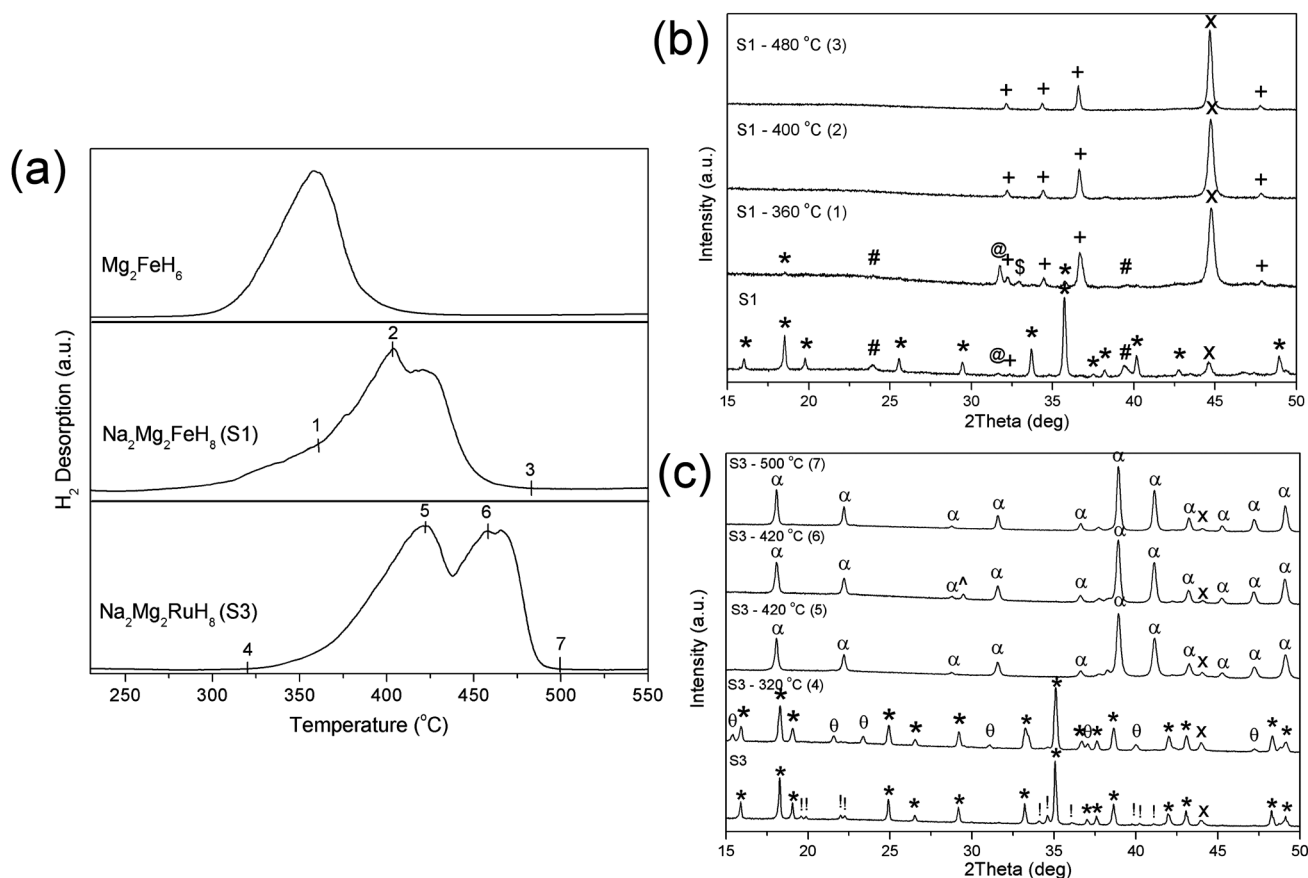
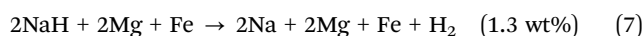
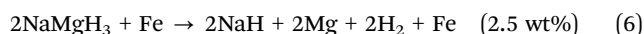
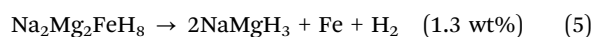


Fig. 2 (a) GC analysis of Mg₂FeH₆, Na₂Mg₂FeH₈ (S1) and Na₂Mg₂RuH₈ (S3) ($\Delta T = 5^\circ\text{C min}^{-1}$). *Ex situ* PXD analysis of (b) Na₂Mg₂FeH₈ (S1) and (c) Na₂Mg₂RuH₈ (S3) at selected temperatures ($\lambda = \text{CuK}\alpha$). Numbers on GC plots correlate to temperatures at which samples were heated prior to PXD analysis. * = Na₂Mg₂TH₈ (T = Fe, Ru); # = Mg₂FeH₆; @ = NaH; x = T (Fe, Ru); \$ = NaMgH₃; ^ = NaOH; + = Mg; α = Mg₃Ru₂; ! = unknown phase; θ = unknown phase.

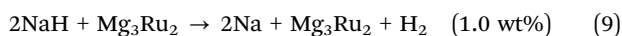


are similar, with two stages of H₂ desorption being observed for both materials (S1 and S3). The onset of decomposition for Na₂Mg₂FeH₈ occurs at *ca.* 280 °C, with the first maxima being observed at *ca.* 400 °C, and the second at *ca.* 430 °C. Decomposition concludes at *ca.* 475 °C. Conversely, the onset of H₂ desorption for Na₂Mg₂RuH₈ occurs at *ca.* 325 °C, with the first maxima being observed at *ca.* 421 °C, and the second at *ca.* 460 °C. H₂ is no longer detected after *ca.* 500 °C.

To ascertain the pathway of decomposition, *ex situ* PXD was conducted on samples heated to selected temperatures *in vacuo* (Fig. 2b and c). Analysis of Na₂Mg₂FeH₈ after heating at 360 °C indicates a minuscule quantity of Na₂Mg₂FeH₈ resides, although the majority has decomposed into NaH, Mg and Fe, while NaMgH₃ is also detected. By 400 °C NaH has decomposed, while only Mg and Fe are observable by PXD. Na is not observed due to the low vapor pressure of Na at elevated temperatures. No further changes to the material are observed at higher temperatures. Therefore the decomposition of Na₂Mg₂FeH₈ is determined to occur according to eqn (5)–(7).



Na₂Mg₂RuH₈ was first heated to 320 °C, where PXD determined that decomposition has not yet started. By 420 °C full decomposition appears to be complete, with Mg₃Ru₂ and Ru being the products. At this temperature, NaH instantly decomposes to Na and evaporates from the sample. As a result, the decomposition of Na₂Mg₂RuH₈ is determined to occur according to eqn (8) and (9). Presumably the excess Ru required to form Mg₃Ru₂ (without leaving excess Mg) comes from the excess Ru that remained in the starting material.



PCI analysis of Na₂Mg₂TH₈ (T = Fe, Ru) (Fig. 3a and b) enables the intricacies of the decomposition process to be truly understood. The experiments on Na₂Mg₂FeH₈ were conducted at initial pressures of 30 MPa and 400 °C, mimicking conditions used for synthesis. Consequently, it was ascertained that the first thermal reaction according to eqn (5), occurs at an equilibrium pressure of 15.5 MPa, releasing *ca.* 0.8 wt% H₂ at 400 °C (Fig. 4a). PXD analysis of the products recovered at 6 MPa characterised the products to be NaMgH₃ and Fe (Fig. 3e). Δ*H*_{dec} for this process was determined by means of a van't Hoff plot of H₂ desorption equilibrium pressures and the linear fit (*R*² = 0.975) to the data to be 93 kJ mol⁻¹ H₂ (Fig. 3c), while the corresponding Δ*S*_{dec} was calculated as 180 J mol⁻¹ H₂/K. However, at lower temperatures this step is kinetically hindered and as a result Δ*H* and Δ*S* may be obscured. The values reported above are an average of the plateau pressures.

The further two equilibrium plateaus below 1 MPa H₂ correspond to the decomposition of NaMgH₃, exhibiting mass losses of 2.5 and 1.5 wt% for eqn (6) and (7), respectively. The overall

hydrogen content released was therefore determined to be 4.7 wt% at 400 °C (theoretical maximum of 5.1 wt%). Δ*H*_{dec} was calculated to be 87 and 111 kJ mol⁻¹ H₂ for the latter two processes, in accord with the literature values.³⁶ The corresponding Δ*S*_{dec} also agreed with literature values with 132 and 158 J mol⁻¹ H₂/K for eqn (6) and (7), respectively. Therefore Δ*H*_{des} for the entire system is surmised to be 378 kJ mol⁻¹ (94.5 kJ mol⁻¹ H₂). The identity of the species at each decomposition stage was determined by PXD by ending selected PCI experiments at specified pressures. Fig. 3e illustrates the final products after the PCI experiments conducted at 360 and 400 °C and also those observed after the first and during the second equilibrium step (eqn (6)). During the second equilibrium step, NaMgH₃, Fe and NaH, and Mg are observed, indicating that NaMgH₃ is decomposing. After the third equilibrium (final products), Na, Mg and Fe are the main constituents, although residual NaH is also observed. Therefore the decomposition process can be described according to eqn (5)–(7) and Fig. 4.

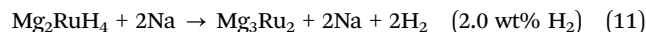
The thermal stability of Na₂Mg₂FeH₈ is enhanced compared to that of Mg₂FeH₆, which exhibits a H₂ desorption maxima at *ca.* 360 °C (Fig. 2) with an associated Δ*H*_{des} of 261 kJ mol⁻¹.²⁹ The additional stability achieved by the incorporation of Na⁺ and H⁻ into the compound, induces a significant increase in desorption temperature maxima to 400 °C and a total Δ*H*_{des} of 378 kJ mol⁻¹ (Fig. 4). This value correlates very well with the previous DFT calculations conducted on this compound, which determined Δ*H*_f to be -328 kJ mol⁻¹.²³

In contrast to Na₂Mg₂FeH₈, Na₂Mg₂RuH₈ is stable above pressures of 0.19 MPa H₂ and *T* > 500 °C (Fig. 3a). PXD analysis of material annealed at 6 MPa H₂ and 450 °C (Fig. 3f) indicates that the only modification is the disappearance of the unknown phase (observed after initial synthesis (Fig. 1)) which is replaced by another unknown phase. This material can be indexed to an orthorhombic unit cell of *a* = 14.5331, *b* = 7.9841 and *c* = 6.2429 and crystallises in a possible space group of *Pmmn*, although structural identification is inhibited by the low concentration and weak intensity of the Bragg peaks. As was observed from the GC results (Fig. 1), decomposition is also noted to follow a two-step decomposition route by PCI. At 500 °C, the first plateau is observed at an equilibrium pressure of 0.19 MPa, while the second occurs at *ca.* 0.07 MPa. Each step was determined to have an associated mass loss of *ca.* 1.9 wt%, with a total of 3.8 wt% H₂ being desorbed out of a maximum theoretical capacity of 4.0 wt%. This process was also carried out at 475 and 450 °C. This allowed for Δ*H*_{des} and Δ*S* to be determined to be 131 kJ mol⁻¹ H₂ and 176 Δ*S* (J mol⁻¹ H₂/K), respectively for step 1 (*R*² = 0.984) and Δ*H*_{des} = 119 kJ mol⁻¹ H₂ and Δ*S* = 151 Δ*S* (J mol⁻¹ H₂/K) for step 2 (*R*² = 0.999) (Fig. 3d). Therefore Δ*H*_{des} for the entire system is surmised to be 500 kJ mol⁻¹ (125 kJ mol⁻¹ H₂). PXD of the products at each stage allows a greater insight into those determined by *ex situ* heating *in vacuo*. After the first plateau, a substantial level of Mg₂RuH₄ is identifiable in the powder, along with Ru, NaOH and a small quantity of Mg₃Ru₂. The highly oxidisable Na (residual after evaporation) is the source of NaOH (occurring during PXD analysis),



while the thermally unstable Mg_2RuH_4 is the source of Mg_3Ru_2 . An unknown phase is also observed at this temperature and pressure, which due to the low intensity of the Bragg peaks associated with this material, indexing and as such, structural refinement was not possible. After the second plateau, the remaining powder consists of Mg_3Ru_2 and Ru. Presumably the excess Ru required to form Mg_3Ru_2 (without leaving excess Mg) comes from the excess Ru that remains in the starting

material (Fig. 1). Therefore the decomposition process can be described according to eqn (10) and (11) and Fig. 4.



The decomposition pathway of these materials differ significantly in that NaMgH_3 is the intermediate for $\text{Na}_2\text{Mg}_2\text{FeH}_8$,

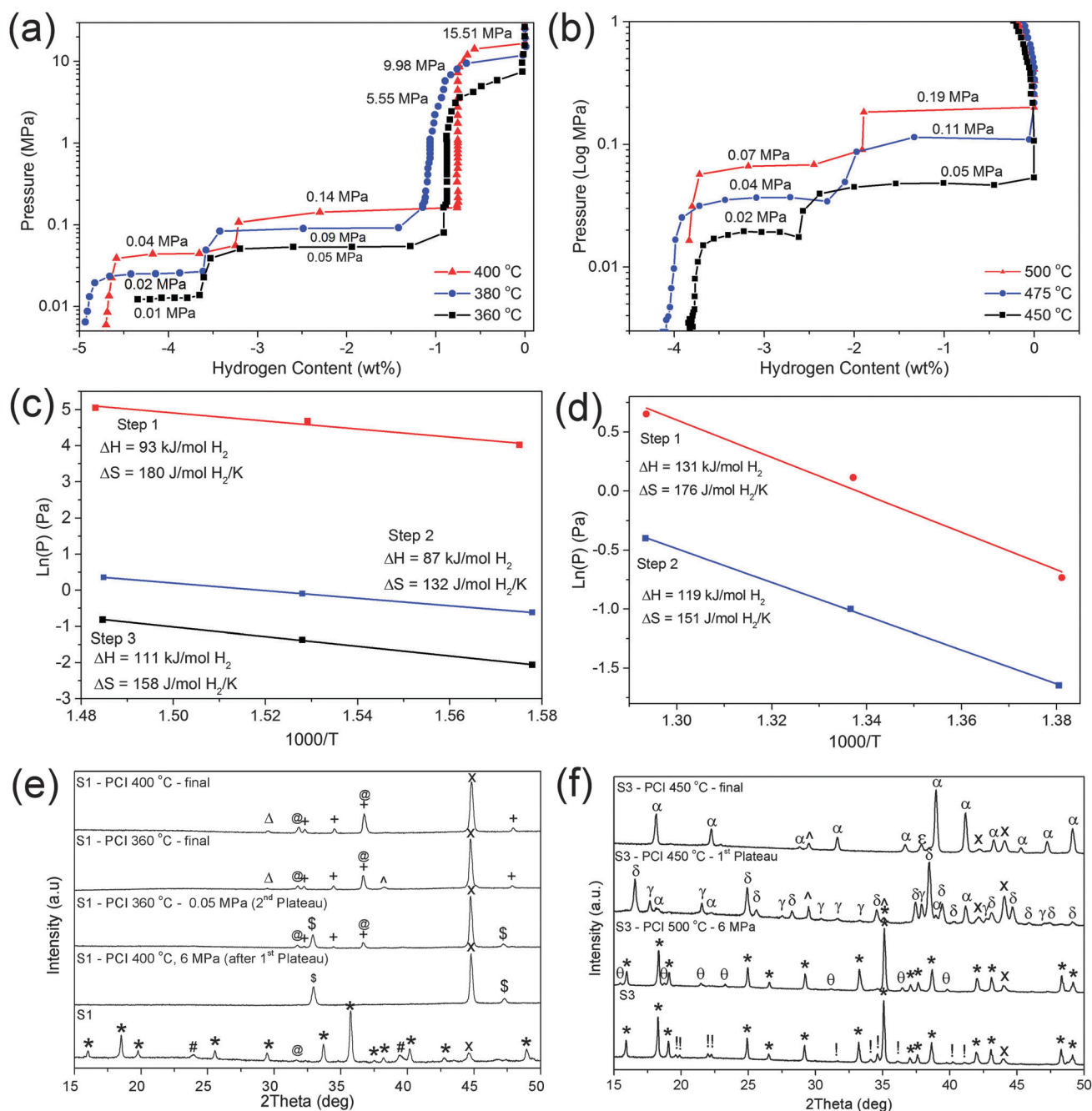


Fig. 3 PCI analysis of $\text{Na}_2\text{Mg}_2\text{FeH}_8$ (a) and $\text{Na}_2\text{Mg}_2\text{RuH}_8$ (b) at selected temperatures. van't Hoff plot of H_2 desorption equilibrium pressures and the linear fit to the data for $\text{Na}_2\text{Mg}_2\text{FeH}_8$ (c) and $\text{Na}_2\text{Mg}_2\text{RuH}_8$ (d). *Ex situ* PXD analysis of $\text{Na}_2\text{Mg}_2\text{FeH}_8$ (S1) (e) and $\text{Na}_2\text{Mg}_2\text{RuH}_8$ (S3) (f) for samples collected after PCI analysis and after rehydrogenation ($\lambda = \text{CuK}\alpha$). * = $\text{Na}_2\text{Mg}_2\text{TH}_8$ (T = Fe, Ru); # = Mg_2FeH_6 ; @ = NaH; x = T (Fe, Ru); \$ = NaMgH_3 ; ^ = NaOH; + = Mg; Δ = Na; α = Mg_3Ru_2 ; δ = Mg_2RuH_4 ; ! = unknown phase; θ = unknown phase; γ = unknown phase; ϵ = unknown phase.



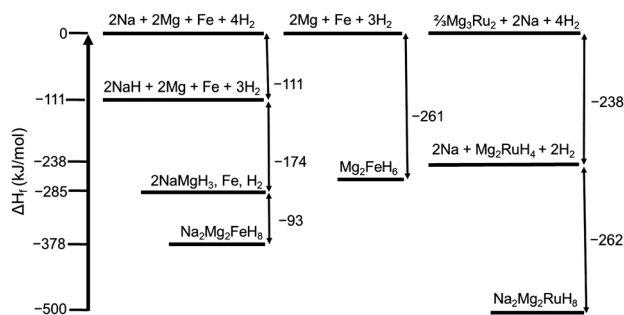


Fig. 4 Energy diagram illustrating the experimentally determined enthalpies of formation (ΔH_{form} , kJ mol^{-1}) of $\text{Na}_2\text{Mg}_2\text{FeH}_8$, Mg_2FeH_6 ,²⁹ and $\text{Na}_2\text{Mg}_2\text{RuH}_8$. The excess Ru required to form Mg_3Ru_2 is acquired from the impurity Ru remaining in the $\text{Na}_2\text{Mg}_2\text{RuH}_8$ starting material.

while $\text{Na}_2\text{Mg}_2\text{RuH}_8$ disassembles *via* Mg_2RuH_4 (Fig. 4). The versatile 4d Ru metal center is known to form a variety of complex anions including $[\text{Ru}_2\text{H}_6]^{12-}$, $[\text{RuH}_4]_n^{4n-}$, $[\text{RuH}_5]_{\text{av}}^{5-}$, $[\text{RuH}_6]^{4-}$ and $[\text{RuH}_7]^{3-}$, while the 3d Fe metal center is only known to form $[\text{FeH}_6]^{4-}$ anions.¹ As a consequence, $\text{Na}_2\text{Mg}_2\text{RuH}_8$ forms the $[\text{RuH}_4]_n^{4n-}$ polyanionic intermediate upon decomposition,³⁷ whereas $\text{Na}_2\text{Mg}_2\text{FeH}_8$ preferentially decomposes to the thermally stable NaMgH_3 ³⁶ rather than Mg_2FeH_6 (Fig. 4). Mg_2RuH_4 was not observed during the *ex situ* heating experiments of $\text{Na}_2\text{Mg}_2\text{RuH}_8$ (Fig. 2e) as it is not thermodynamically stable at the temperatures at which $\text{Na}_2\text{Mg}_2\text{RuH}_8$ decomposes (420 °C, *in vacuo*).³⁷ Although, the synthesis of Mg_2RuH_4 is accomplished at 450 °C under 0.2 MPa H_2 , it would presumably decompose at the temperatures imposed here, especially *in vacuo*. Stabilisation of this species is therefore viable under H_2 pressures of 0.05–0.02 MPa.

Conclusions

The optimised syntheses of $\text{Na}_2\text{Mg}_2\text{TH}_8$ (T = Fe, Ru) have been reported. Ball milling of stoichiometric quantities of NaH, MgH_2 and Fe followed by hydrogenation allows for a yield of >90% purity of $\text{Na}_2\text{Mg}_2\text{FeH}_8$ *via* the formation of a NaMgH_3 intermediate. On the contrary, no intermediate is observed during the synthesis of $\text{Na}_2\text{Mg}_2\text{RuH}_8$ using an identical procedure.

The thermal decomposition of both $\text{Na}_2\text{Mg}_2\text{TH}_8$ materials have been studied by *ex situ* PXD, GC and PCI measurements. The first desorption maxima of $\text{Na}_2\text{Mg}_2\text{FeH}_8$ has been established to occur at *ca.* 400 °C, while $\text{Na}_2\text{Mg}_2\text{RuH}_8$ has its first maxima at 420 °C. The decomposition pathways of these isostructural compounds differs considerably, with $\text{Na}_2\text{Mg}_2\text{FeH}_8$ proceeding *via* NaMgH_3 in a three-step process, while $\text{Na}_2\text{Mg}_2\text{RuH}_8$ decomposes *via* Mg_2RuH_4 in a two-step process. The dissimilarity between the pathways originates from the capability of the 4d Ru metal centre to exist in a variety of $[\text{RuH}_x]^{n-}$ complexes compared to Fe, which only exists as $[\text{FeH}_6]^{4-}$.

The enthalpy and entropy of desorption for $\text{Na}_2\text{Mg}_2\text{TH}_8$ (T = Fe, Ru) for each stage of decomposition has been established to be by PCI measurements. The total enthalpy of desorption for

$\text{Na}_2\text{Mg}_2\text{FeH}_8$ is 95 kJ mol^{-1} H_2 and 125 kJ mol^{-1} H_2 for $\text{Na}_2\text{Mg}_2\text{RuH}_8$.

Acknowledgements

We would like to acknowledge Ms. Warifune for the synthesis of the Mg_2FeH_6 starting material. We also appreciate the financial support from JSPS KAKENHI Grant Number 25220911.

Notes and references

- 1 K. Yvon and G. Renaudin, *Encyclopedia of Inorganic Chemistry*, John Wiley & Sons, Ltd, 2006.
- 2 K. Yvon, *Chimia*, 1998, **52**, 613–619.
- 3 J. J. Reilly and R. H. Wiswall, *Inorg. Chem.*, 1968, **7**, 2254–2256.
- 4 H. Blomqvist and D. Noréus, *J. Appl. Phys.*, 2002, **91**, 5141–5148.
- 5 M. Lelis, D. Milcius, E. Wirth, U. Halenius, L. Eriksson, K. Jansson, K. Kadir, J. Ruan, T. Sato, T. Yokosawa and D. Noréus, *J. Alloys Compd.*, 2010, **496**, 81–86.
- 6 R. J. Westerwaal, M. Slaman, C. P. Broedersz, D. M. Borsa, B. Dam, R. Griessen, A. Borgschulte, W. Lohstroh, B. Kooi, G. ten Brink, K. G. Tschersich and H. P. Fleischhauer, *J. Appl. Phys.*, 2006, **100**, 063518.
- 7 T. J. Richardson, J. L. Slack, R. D. Armitage, R. Kostecki, B. Farangis and M. D. Rubin, *Appl. Phys. Lett.*, 2001, **78**, 3047–3049.
- 8 M. Polanski, T. K. Nielsen, Y. Cerenius, J. Bystrzycki and T. R. Jensen, *Int. J. Hydrogen Energy*, 2010, **35**, 3578–3582.
- 9 M. Polanski, K. Witek, T. K. Nielsen, L. Jaroszewicz and J. Bystrzycki, *Int. J. Hydrogen Energy*, 2013, **38**, 2785–2789.
- 10 J. J. Didisheim, P. Zolliker, K. Yvon, P. Fischer, J. Schefer, M. Gubelmann and A. F. Williams, *Inorg. Chem.*, 1984, **23**, 1953–1957.
- 11 G. Li, M. Matsuo, S. Deledda, R. Sato, B. C. Hauback and S. Orimo, *Mater. Trans.*, 2013, **54**, 1532–1534.
- 12 T. J. Richardson, J. L. Slack, B. Farangis and M. D. Rubin, *Appl. Phys. Lett.*, 2002, **80**, 1349–1351.
- 13 B. Bogdanović, A. Reiser, K. Schlichte, B. Spliethoff and B. Tesche, *J. Alloys Compd.*, 2002, **345**, 77–89.
- 14 S. F. Parker, K. P. J. Williams, M. Bortz and K. Yvon, *Inorg. Chem.*, 1997, **36**, 5218–5221.
- 15 B. Huang, K. Yvon and P. Fischer, *J. Alloys Compd.*, 1995, **227**, 121–124.
- 16 B. Huang, F. Gingl, F. Fauth, A. Hewat and K. Yvon, *J. Alloys Compd.*, 1997, **248**, 13–17.
- 17 B. Huang, K. Yvon and P. Fischer, *J. Alloys Compd.*, 1994, **204**, 5–8.
- 18 G. Renaudin, L. Guenee and K. Yvon, *J. Alloys Compd.*, 2003, **350**, 145–150.
- 19 M. Orlova, J.-P. Rapin and K. Yvon, *Inorg. Chem.*, 2009, **48**, 5052–5054.



- 20 T. D. Humphries, S. Takagi, G. Li, M. Matsuo, T. Sato, M. H. Sørby, S. Deledda, B. C. Hauback and S. Orimo, *J. Alloys Compd.*, 2015, DOI: 10.1016/j.jallcom.2014.12.113.
- 21 M. Matsuo, H. Saitoh, A. Machida, R. Sato, S. Takagi, K. Miwa, T. Watanuki, Y. Katayama, K. Aoki and S. Orimo, *RSC Adv.*, 2013, **3**, 1013–1016.
- 22 H. Saitoh, S. Takagi, M. Matsuo, Y. Iijima, N. Endo, K. Aoki and S. Orimo, *APL Mater.*, 2014, **2**, 076103.
- 23 S. Takagi, T. D. Humphries, K. Miwa and S. Orimo, *Appl. Phys. Lett.*, 2014, **104**, 203901.
- 24 M. Di Chio, L. Schiffini, S. Enzo, G. Cocco and M. Baricco, *J. Alloys Compd.*, 2007, **434**, 734–737.
- 25 K. Kadir and D. Noréus, *Inorg. Chem.*, 2007, **46**, 3288–3289.
- 26 B. Huang, K. Yvon and P. Fischer, *J. Alloys Compd.*, 1992, **187**, 227–232.
- 27 B. Huang, K. Yvon and P. Fischer, *J. Alloys Compd.*, 1992, **190**, 65–68.
- 28 B. Huang, K. Yvon and P. Fischer, *J. Alloys Compd.*, 1993, **197**, 65–68.
- 29 J. A. Puszkiel, P. Arneodo Larochette and F. C. Gennari, *J. Alloys Compd.*, 2008, **463**, 134–142.
- 30 A. Boulitif and D. Louer, *J. Appl. Crystallogr.*, 2004, **37**, 724–731.
- 31 J. Laugier and B. Bochu, LMGP-Suite Suite Programs Interpret. X-ray Exp. by Jean laugier Bernard Bochu, ENSP/Laboratoire des Matériaux du Génie Phys. BP 46. 38042 Saint Martin d'Hères, Fr.
- 32 B. H. Toby, *J. Appl. Crystallogr.*, 2001, **34**, 210–213.
- 33 A. C. Larson and R. B. Von Dreele, *Los Alamos National Laboratory Report*, 2000, LAUR 86-748.
- 34 B. E. Warren, *X-ray Diffraction*, Courier Dover Publications, 1969.
- 35 H. Reardon, N. Mazur and D. H. Gregory, *Prog. Nat. Sci.*, 2013, **23**, 343–350.
- 36 D. A. Sheppard, M. Paskevicius and C. E. Buckley, *Chem. Mater.*, 2011, **23**, 4298–4300.
- 37 F. Bonhomme, K. Yvon, G. Triscone, K. Jansen, G. Auffermann, P. Müller, W. Bronger and P. Fischer, *J. Alloys Compd.*, 1992, **178**, 161–166.

